



HAL
open science

Neptunium sorption and redox speciation at the illite surface under highly saline conditions

Nidhu Lal Banik, Remi Marsac, Johannes L Lützenkirchen, Christian Michael Maquardt, Kathy Dardenne, Joerg Rothe, Kerstin Bender, Horst Geckeis

► To cite this version:

Nidhu Lal Banik, Remi Marsac, Johannes L Lützenkirchen, Christian Michael Maquardt, Kathy Dardenne, et al.. Neptunium sorption and redox speciation at the illite surface under highly saline conditions. *Geochimica et Cosmochimica Acta*, 2017, 215, pp.421-431. <10.1016/j.gca.2017.08.008>. <insu-01588250>

HAL Id: insu-01588250

<https://insu.hal.science/insu-01588250v1>

Submitted on 15 Sep 2017

HAL is a multi-disciplinary open access archive for the deposit and dissemination of scientific research documents, whether they are published or not. The documents may come from teaching and research institutions in France or abroad, or from public or private research centers.

L'archive ouverte pluridisciplinaire **HAL**, est destinée au dépôt et à la diffusion de documents scientifiques de niveau recherche, publiés ou non, émanant des établissements d'enseignement et de recherche français ou étrangers, des laboratoires publics ou privés.



HAL Authorization

1 **Neptunium sorption and redox speciation at**
2 **the illite surface under highly saline**
3 **conditions**
4
5

6 Nidhu lal Banik^{a,b}, Rémi Marsac^{a,c,*}, Johannes Lützenkirchen^a, Christian Michael Marquardt^a,
7 Kathy Dardenne^a, Joerg Rothe^a, Kerstin Bender^a and Horst Geckeis^a
8
9
10

11 Address:

12 ^a Institut für Nukleare Entsorgung, Karlsruhe Institute of Technology, P.O. Box 3640, D-
13 76021 Karlsruhe, Germany.
14

15 Present addresses:

16 ^b JRC-KARLSRUHE, G.II.6 - Nuclear Safeguards and Forensics, European Commission, P.O.Box
17 2340, D-76125 Karlsruhe

18 ^c Géosciences Rennes UMR 6118, Université Rennes 1, CNRS, 35042 Rennes cedex, France.
19
20
21

22 *Corresponding author:

23 e-mail address: remi.marsac@univ-rennes1.fr

24 Tel: +332 23 23 53 56. Fax: +332 23 23 60 90
25

26 **ABSTRACT.** Neptunium (Np) uptake on illite is investigated in 1 and 3.2 molal (m) NaCl
27 solutions under inert (Ar) atmosphere for $4 < \text{pH}_m < 10$ ($\text{pH}_m = -\log m_{H^+}$) and $5 \times 10^{-8} <$
28 $[\text{Np(V)}]_{\text{tot}} < 3 \times 10^{-4}$ M. In agreement with a previous study in 0.1 m NaCl solutions [Marsac et
29 al. (2015) *Geochim. Cosmochim. Acta* 152, 39-51], Np(V) is the prevailing oxidation state in
30 the aqueous solution, but Np uptake by illite is affected by surface induced reduction. The
31 extent of Np(V) reduction to Np(IV) follows the measured redox potential (or the $\text{pe} = -\log$
32 a_e), which is influenced by the introduced Np(V) amount, because of the low redox capacity
33 of the illite. The presence of Np(IV) on the solid phase is verified by X-ray Absorption Near
34 Edge Spectroscopy (XANES). We can conclude that Np uptake by illite is not significantly
35 affected by the variation of m_{NaCl} from 0.1 to 3.2 m and thus is in agreement with reports on
36 tetravalent actinide and Np(V) sorption to clays at high ionic strength. The combination of (i)
37 the two site protolysis non-electrostatic surface complexation and cation exchange model, (ii)
38 the specific ion interaction theory to calculate activity coefficients for dissolved species and
39 (iii) by accounting for redox equilibria and the stability of surface Np species, the overall Np
40 uptake by illite can be simulated as a function of pH_m , pe and m_{NaCl} using a single set of
41 parameters. The present experimental and modeling results are particularly important in the
42 context of deep geological nuclear waste disposal since many sedimentary rocks or clay
43 formations that are deemed suitable for this purpose exhibit highly saline porewaters.

44 Keywords: Neptunium, illite, redox, saline, high ionic strength, surface complexation,
45 spectroscopy, geochemical modeling.

1. INTRODUCTION

47 The final disposal in deep geologic formations is considered the most appropriate
48 strategy to isolate high level nuclear waste (HLW) from the biosphere (e.g. OECD/NEA,
49 2008). Sedimentary clay rock formations are potential host rocks for HLW in several
50 European countries encompassing Opalinus Clay (OPA) in Switzerland (Nagra, 2002), Boom
51 and Ypresian clays in Belgium (Ondraf, 2001), Callovo-Oxfordian (COx) clays in France
52 (Andra, 2005) or Boda Claystone in Hungary (Lázár and Máthé, 2012). Indeed, clays exhibit
53 low permeability, large surface areas and pronounced sorption capacity for many relevant
54 radionuclides via ion exchange reactions as well as surface complexation to silanol and/or
55 aluminol groups at the edges of clay particles. Illite and smectite are the most important
56 components of the proposed claystone host rocks and may amount to about 50 wt.% of the
57 material (Lauber et al., 2000; Gaucher et al., 2004; Bradbury and Baeyens, 2011; Pearson et
58 al., 2011; Chen et al., 2014). Although actinide sorption to clays has been extensively studied
59 (e.g. Bradbury and Baeyens, 2005; 2009a,b; and references therein), the underlying
60 mechanisms were rarely investigated for ionic strengths above 0.1 M. While OPA and COx
61 porewaters exhibit ionic strengths of 0.3-0.4 M, clay rock pore waters as e.g. in the Jurassic
62 and lower Cretaceous clay rock in Northern Germany, which are also discussed as
63 potentially appropriate host rock formations, may contain salt contents as high as about 5 M
64 (Brewitz, 1980). Sedimentary rocks currently investigated in Canada are even in contact with
65 brine solutions up to 6.5 M (Fritz and Frape, 1982). Therefore, detailed sorption investigations
66 and the development of geochemical models that can predict actinide sorption and speciation
67 in concentrated brine solutions are required (Vilks, 2011).

68 Neptunium (Np) is a minor constituent of high level radioactive waste. Yet, its
69 environmental chemistry is of considerable interest due to the long half-life of its main
70 isotope ^{237}Np ($t_{1/2} = 2 \times 10^6$ a) and the high solubility and mobility of its pentavalent state

71 (NpO₂⁺) under oxidizing conditions. Np is redox sensitive and its most relevant oxidation
72 states in the geosphere are the penta- and tetravalent states (Kim, 1986). Both redox states
73 show drastically different geochemical behavior concerning, for instance, complexation by
74 organic and inorganic ligands, solubility, as well as sorption to minerals (e.g. Altmaier et al.,
75 2013). Under reducing conditions, Np(IV) prevails and is considered rather immobile because
76 of its strong sorption to minerals and its low solubility, as other tetravalent actinides (An; e.g.
77 Th(IV)) or other tetravalent elements (e.g. Sn(IV)) (Bradbury and Baeyens, 2009a,b). Under
78 oxidizing conditions, Np(V) prevails, which weakly sorbs to minerals and is regarded as
79 rather mobile (e.g. Geckeis et al., 2013). However, partial reduction of Np(V) to Np(IV) when
80 in contact with Opalinus Clay was suggested by comparing sorption data obtained under
81 aerobic and anaerobic conditions: stronger Np sorption (Fröhlich et al., 2011) was found
82 under anaerobic conditions and significant reduction to Np(IV) was observed using
83 synchrotron based spectroscopic techniques (Fröhlich et al., 2012). A more recent Np-illite
84 batch sorption study under oxygen-free argon atmosphere in 0.1 M NaCl showed that the
85 strongly adsorbing Np(IV) is thermodynamically favored at a mineral surface compared to
86 Np(V) (Marsac et al., 2015a). Although Np(V) prevailed in aqueous solution at pH ≈ 7, as
87 evidenced by liquid-liquid extraction method and by capillary electrophoresis hyphenated to
88 inductively coupled plasma mass spectrometry (Graser et al., 2015), Np(IV) was observed at
89 the illite surface by X-ray absorption near edge structure spectroscopy (XANES). When
90 accounting for the uptake of both Np(V) and Np(IV) on illite and the redox potential of the
91 illite suspension, Marsac et al. (2015a) were able to describe the overall Np uptake on illite
92 for various redox conditions. The modeling approach was subsequently extended to the
93 sorption behavior of plutonium, which exhibits an even more complex redox chemistry than
94 Np. Pu can be found in the redox states +III to +VI under environmental conditions. The
95 experimentally determined overall Pu uptake on kaolinite (Marsac et al., 2015b) and illite
96 (Banik et al., 2016) in 0.1 M NaCl/ClO₄ was successfully reproduced.

97 The above cited studies focused on aqueous solutions of low ionic strength. At high
98 salt concentrations, activity coefficients of aqueous species change dramatically, whereas the
99 effect of high ionic strengths on the surfaces properties of adsorbents and surface species is
100 elusive. Previous work showed that non-electrostatic models are quite suitable to predict
101 proton and metal ion sorption at high ionic strength to naturally occurring matrices that bear
102 surface functional groups that are affected by pH and can be treated by the same formalism
103 and with similar numerical models. This includes marine microalgae (Schjif and Herbling,
104 2010; Zoll and Schjif, 2012) or bacteria (Ams et al., 2013). Eu(III) sorption to illite and
105 smectite was investigated experimentally in $0.1 < m_{NaCl} < 3.9$ molal (m) (Schnurr et al.,
106 2015). The results obtained in the latter study showed that the 2 site protolysis non-
107 electrostatic surface complexation and cation exchange (2 SPNE SC/CE) model coupled to
108 either the specific ion interaction theory (SIT; Ciavatta, 1980) or the Pitzer formalism (Pitzer,
109 1991) to account for activity coefficients in concentrated media was able to reproduce
110 sorption data also at elevated ionic strength. By using the modeling approach of Schnurr et al.
111 (2015), the Pu-illite study in 0.1 M NaCl of Banik et al. (2016) was extended to high ionic
112 strength ($0.1 < m_{NaCl} < 3.2$ m; Marsac et al., 2017). In the latter studies, the Pu(IV)/Pu(III) is
113 involved. The present study is a similar extension of the work of Marsac et al. (2015a) on Np
114 uptake on illite in 0.1 M NaCl to highly saline conditions (up to $m_{NaCl} = 3.2$ m), but here a
115 An(V)/An(IV) couple is involved. Together, the work of Marsac et al. (2017) and the present
116 one should elucidate the actinide(III,IV,V) sorption and redox speciation at the illite surface
117 under highly saline conditions. Classical batch experiments at various pH, total Np
118 concentrations and $m_{NaCl} = 1.0$ and 3.2 m were performed, and the redox potential was
119 monitored. XANES was applied to determine the Np redox state at the illite surface. The
120 coupling of the 2 SPNE SC/CE model with SIT was used to describe Np sorption and redox
121 speciation on illite under saline conditions.

122

123

2. MATERIALS AND METHODS

124 All chemicals were of pro analytical quality or better and were obtained from Merck
125 (Darmstadt, Germany) or Riedel de Haen (Seelze, Germany). Experiments were conducted
126 with de-ionized “MilliQ” water (specific resistivity, 18.2 MΩ cm). The purified Na-illite was
127 provided within the EC project CP CatClay. The source material derives from lacustrine
128 continental sediments deposited at the Upper Eocene (~ -35 Ma) in the basin of Le Puy en
129 Velay (Massif Central, France). The purification procedures and the characterization of the
130 purified illite (<63 μm) were previously described in detail (Marsac et al., 2015). Concerning
131 redox processes, it is noted that the iron content is 0.88 mol Fe per kg of illite (Marsac et al.,
132 2015). The aqueous concentration of ^{237}Np in sorption experiments after phase separation was
133 determined by liquid scintillation counting (LSC) using the scintillation cocktail Ultima Gold
134 XR (Packard Instruments Co., USA) and the liquid scintillation counter (LSC) Tri-Carb
135 (Packard Instruments Co., USA). Results for ^{237}Np - α -activities were corrected for
136 interferences by the β -radiation from the daughter nuclide protactinium (^{233}Pa) by applying
137 the α/β discrimination method. The procedure is described in detail by Marsac et al. (2015a)
138 and will not be repeated here. ^{233}Pa is a short-lived isotope ($t_{1/2} = 27$ days) unlike ^{237}Np ($t_{1/2} =$
139 $2.14 \cdot 10^6$ years). Since the ^{233}Pa mass concentration is much smaller than that of ^{237}Np , its
140 competitive effect on Np sorption to illite can be neglected.

141

142 2.1. Neptunium stock solution

143 The initial ^{237}Np solution was evaporated to dryness and dissolved in 8 M HCl. The
144 solution was purified via anion exchange (BIO RAD[®] AG 1-X8). After a washing step with
145 several milliliters of 8 M HCl, Pu contaminations were removed with a fresh solution of 150
146 mg NH₄I in 5 mL 8 M HCl. Subsequently, Np was eluted from the ion exchanger with 4 M
147 HCl/0.05 M HF and evaporated to dryness in a PTFE beaker. The sample was fumed twice

148 with 1 M HClO₄ and the residue was dissolved in deionized water to obtain a solution
149 containing only NpO₂⁺, as required for all our experiments, and its purity was verified by UV-
150 Vis/NIR spectroscopy (Sjoblom and Hindman 1951). The final Np concentration was
151 determined by LSC.

152 **2.2. Determination of pH and Eh**

153 pH in the clay suspensions was measured by an Orion 525A pH meter and a Ross electrode
154 calibrated with 4 standard buffers (pH 3, 5, 7 and 9; Merck). The uncertainty of pH
155 measurements is ± 0.05. For converting the pH value measured in saline solutions (I > 0.1 m)
156 (pH_{exp}) into a chemically meaningful quantity, a correction is applied in order to obtain the
157 molal proton concentration, i.e. -log m_{H+} (pH_m). An empirical correction coefficient (A)
158 which has been accurately determined by Altmaier et al. (2003) for NaCl solutions for our set-
159 up with known -log m_{H+} was added to pH_{exp} values according to equations 1 and 2:

$$160 \quad pH_m = pH_{exp} + A_{NaCl} \quad (1)$$

$$161 \quad A_{NaCl} = 0.0013 \times m_{NaCl}^2 + 0.1715 \times m_{NaCl} - 0.0988 \quad (2)$$

162 where m_{NaCl} is the molality (mol kg⁻¹) of the background electrolyte.

163 The redox potentials in the clay suspensions were measured using an Orion 525A (E_h
164 meter) and a Pt combined electrode with a Ag/AgCl reference (Metrohm). They were
165 converted into Eh vs. standard hydrogen electrode (SHE) by correcting for the potential of the
166 reference electrode. A commercial redox-buffer (220 mV, Schott instruments) was used for
167 calibration. An equilibration time of 15 min was allowed for all Eh measurements, after
168 having stirred the suspension. Uncertainties in Eh measurements are ± 50 mV (Altmaier et al.,
169 2010; Kirsch et al., 2011). Eh was converted to the logarithm of the apparent electron activity,
170 $pe = -\log a_e = 16.9 \times Eh(V)$ at 25°C. To our best knowledge, no ionic strength dependent
171 correction needs to be performed for experimentally measured Eh values (as the one that has
172 been described for pH measurements in brines above).

173 2.3. Batch sorption experiments

174 All sorption experiments were performed as batch type experiments with initial Np(V)
175 concentrations in the range of 5×10^{-8} - 3×10^{-6} M. The batch experiments were carried out in 40
176 mL polypropylene centrifuge tubes at room temperature in an argon glove box (< 1 ppm O₂,
177 absence of CO₂). The sample volume was 25 mL. At a solid-to-liquid ratio of 2 g L⁻¹, the
178 suspensions were preconditioned at a given m_{NaCl} under continuous shaking for 4-5 days to
179 achieve a given target pH_m value by adding 0.1 M HCl or 0.1 M NaOH. After mixing the
180 NpO₂⁺ solution with the preconditioned illite suspension, pH_m was readjusted by adding acid
181 or base (HCl/NaOH). The samples were shaken end-over-end. According to Marsac et al.
182 (2015a), Np(V) adsorption or reduction to Np(IV) does not significantly change with time
183 after 7 days. Therefore, after 7 days, pH_m and Eh were measured in the suspension and an
184 aliquot of each sample was centrifuged in a Beckman L7 Ultracentrifuge at 90000 rpm for 1 h.
185 The supernatant was analyzed for dissolved Np by LSC. Results obtained in batch
186 experiments will be expressed throughout as distribution coefficients (R_d in L kg⁻¹), calculated
187 by the following equation:

$$188 R_d = ([Np]_{tot}/[Np]_{aq} - 1) \times V/m \quad (3)$$

189 where $[Np]_{aq}$ and $[Np]_{tot}$ (mol L⁻¹) are the dissolved (final) equilibrium and total (initial)
190 concentrations of Np in solution, respectively. The term V/m corresponds to the aqueous
191 solution volume to illite mass ratio (L kg⁻¹). An uncertainty of ± 0.3 is commonly associated
192 with log R_d determined for radionuclide sorption to clay minerals (Bradbury and Baeyens,
193 2009a), although for low $[Np]_{tot}$ and high uptake, the uncertainty on log R_d might be larger.

194 2.4. X-ray absorption near-edge spectroscopy (XANES)

195 One sample was prepared as described in the previous section for Np L₃-XANES
196 measurements for $[NpO_2^+]_{tot} = 3 \times 10^{-4}$ M, $m/V = 20$ g L⁻¹, $m_{NaCl} = 3.2$ and pH_m = 7.9 under

197 inert (Ar) atmosphere. The Eh measured after one week equilibration time was 0.43 ± 0.05 V
198 ($pe = 7.3 \pm 0.8$). A similar experiment is described in Marsac et al. (2015a), however,
199 performed in 0.1 m NaCl and at $Eh = 0.40 \pm 0.05$ V ($pe = 6.8 \pm 0.8$). Conditions for XANES
200 measurements and the data treatment were identical to what has been described in detail in
201 Marsac et al. (2015a). Briefly, an aliquot was centrifuged at 3000 g in a polyethylene vial
202 (500 μ L). The supernatant was discarded, but an aliquot was taken for LSC. The wet illite
203 paste was transferred into a vial, mounted inside an Ar-flushed cell, which acts as a second
204 containment and keeps the sample vials in an anaerobic atmosphere (Brendebach et al., 2009).
205 Measurements were performed at the 2.5 GeV synchrotron light source ANKA, KIT,
206 Germany, at the INE-Beamline for actinide research (Rothe et al., 2006; 2012). A pair of
207 Ge(422) crystals was used in the Lemonnier-type double crystal monochromator (DCM). The
208 monochromatic radiation is focused by a Rh-coated toroidal mirror to a spot of $< 1 \text{ mm} \times 1$
209 mm at the sample position. Higher harmonic radiation in the incident beam was suppressed by
210 detuning the parallel alignment of the DCM crystals to 70 % of photon flux peak intensity in
211 the middle of the spectral range at the beginning of each scan. The incident flux was measured
212 by an Ar-filled ionization chamber at ambient pressure and held constant by a digital
213 MOSTAB feedback system. The Np L_3 -edge spectra ($E(\text{Np}^0 2p_{3/2}) = 17.61$ keV) were
214 calibrated against the first derivative XANES spectrum of a Zr foil (energy of the first
215 inflection point set to $E(\text{Zr}^0 1s) = 17.998$ keV). All Np L_3 -XANES spectra were recorded in
216 fluorescence detection mode by registering the Np L_α fluorescence yield at ~ 13.95 keV as a
217 function of the incident photon energy with a 5-pixel Ge solid state detector (Canberra LEGe).
218 Up to 5 scans were collected at room temperature and averaged for each sample. The
219 illuminated area of the sample was changed between each scan to minimize potential Np
220 redox reactions induced by the beam. XANES spectra were extracted following subtraction of
221 a linear pre-edge background function and normalization of the edge jump to unity using the
222 Demeter Athena software (Ravel and Newville, 2005). The same energy range was

223 considered for the pre-edge and for the normalization of all XANES spectra (pre-edge: 17.30-
224 17.55 keV; post-edge: 17.77-18.20 keV). Preliminary tests ensured that the differences in the
225 XANES were not due to the normalization procedure.

226

227 2.5. Thermodynamic modeling

228 pe-pH diagrams for Np were obtained using PhreePlot (Kinniburgh and Cooper,
229 2009), which contains an embedded version of the geochemical speciation program
230 PHREEQC (Parkhurst and Appelo, 1999). PhreePlot also includes a parameter optimization
231 procedure, which allows fitting a model to experimental data by minimizing the weighted sum
232 of squares of the residuals. Thermodynamic constants for Np aqueous speciation were taken
233 from the NEA thermodynamic database (Guillaumont et al., 2003). The specific ion
234 interaction theory (SIT; Ciavatta, 1980) was used for the calculation of the activity
235 coefficients of aqueous species. The 2 SPNE SC/CE model was used to simulate Np sorption
236 to illite (Bradbury and Baeyens, 2009b). Cation exchange reactions of a metal ion with a
237 charge +n (M^{n+}) on Na-illite can be written as follows (Gaines and Thomas, 1953):



239 The cation exchange capacity (CEC) of the illite was set to 0.225 eq/kg. Surface complexation
240 reactions can be written as follows:



242 where M^{n+} is a metal ion with a charge of +n and $\equiv \text{SOH}$ is a protonated surface site.

243 Only the least abundant, i.e. strong, sites of the 2 SPNE SC/CE model were considered in the
244 adsorption calculations with a site density of $2 \times 10^{-3} \text{ mol kg}^{-1}$, since the weak sites are
245 irrelevant at trace levels of Np. Bradbury and Baeyens (2009b) determined a $\text{NpO}_2^+ \text{-Na}^+$
246 selectivity coefficient for illite as well as Np(V) surface complexation constants for illite
247 within the 2 SPNE SC/CE model. Marsac et al. (2015a) determined surface complexation

248 constants for Np(IV). However, the fitted constants relied on the experimental Eh and,
249 therefore, are subject to large uncertainties. Np and Pu are neighbors in the actinide series and
250 the hydrolysis constants of Np(IV) and Pu(IV) are not significantly different (Guillaumont et
251 al., 2003). On the basis of the linear free energy relationship determined for illite by Bradbury
252 and Baeyens (2009b), the surface complexation constant for Np(IV) and Pu(IV) should not
253 significantly differ. Recently, the surface complexation constants for Pu(IV) were refined for
254 illite by Banik et al. (2016). The constants from the latter study were used here for Np(IV).
255 No constants are available for Np(V) and Np(IV) surface complexation to the more abundant
256 but weaker sites defined in the 2 SPNE SC/CE model. The complete aqueous thermodynamic
257 database, SIT coefficients and the parameters for the 2SPNE SC/CE model are given in the
258 supporting information.

259

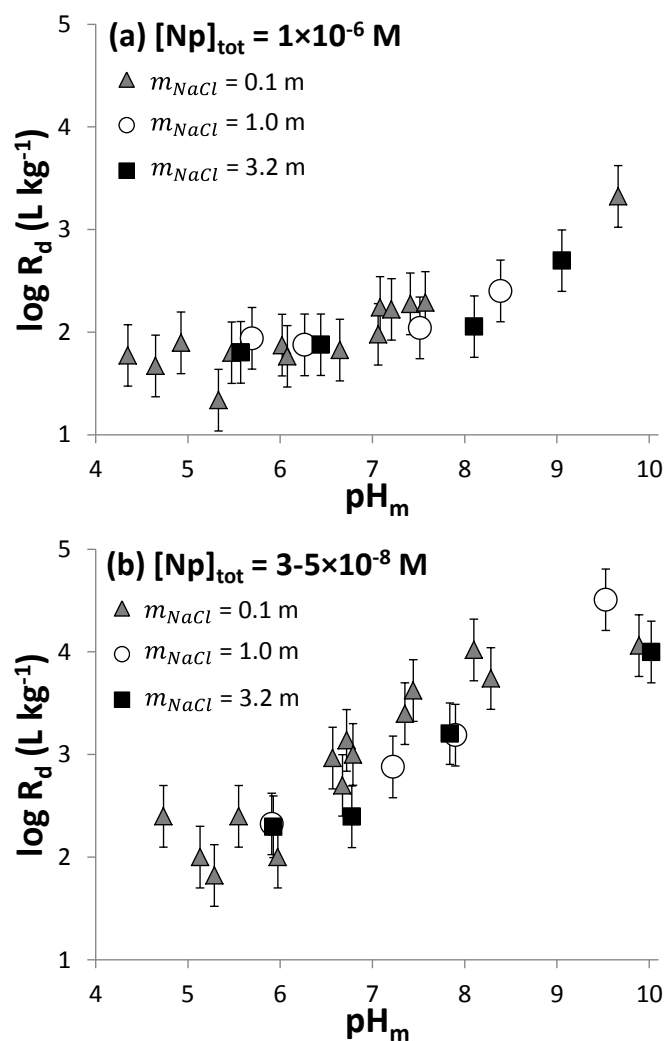
260

3. RESULTS

261 *3.1. Experimental batch results*

262 Figure 1 presents experimental $\log R_d$ (R_d in $L\ kg^{-1}$) values versus pH_m for initial
263 Np(V) concentrations of 10^{-6} M (Fig. 1a) and 5×10^{-8} M (Fig. 1b), and $m_{NaCl} = 1.0$ and 3.2 m.
264 The results of Marsac et al. (2015a) in 0.1 m NaCl obtained after 1 week contact time are
265 included for $[Np(V)]_{tot} = 10^{-6}$ M (Fig. 1a) and 3×10^{-8} M (Fig. 1b). No data are available for
266 $[Np(V)]_{tot} = 5 \times 10^{-8}$ M in 0.1 m NaCl. For both values of $[Np(V)]_{tot}$, no clear effect of the ionic
267 strength on Np sorption is observed. This is consistent with the results of experiments related
268 to the sorption of Np(V) onto illite, shale and bentonite (MX80) in NaCl/CaCl₂ solutions up to
269 I~4.7 M (Nagasaki et al., 2016). For $[Np(V)]_{tot} = 10^{-6}$ M, $\log R_d$ slightly increases with pH_m
270 whereas, for $[Np(V)]_{tot} = 3$ or 5×10^{-8} M, the increase in $\log R_d$ with pH_m is more pronounced.
271 As observed by Marsac et al. (2015a), Np sorption to illite is stronger for low $[Np(V)]_{tot}$. By
272 comparison with the uptake of other cations on illite, it was demonstrated that this behavior

273 cannot be due to site saturation effects (see Figure 2 and corresponding text in Marsac et al.,
274 2015a). In 0.1 m NaCl, the observations for Np were explained by the relatively low p_e
275 measured in the suspension and the formation of Np(IV) at the illite surface, with Np(V)
276 prevailing in the aqueous solution. By addition of 10^{-6} M Np(V) the overall concentration of
277 oxidants in the suspension increases and apparently overcompensates the relatively low redox
278 capacity of the illite suspension. As a consequence, p_e increases and a smaller fraction of
279 Np(V) is reduced to Np(IV), which explains the observed reduced Np uptake at high
280 $[\text{Np(V)}]_{\text{tot}}$. Our results must be interpreted by taking into account the actual redox conditions
281 in the system. Figure 2 shows the complete datasets for various $[\text{Np(V)}]_{\text{tot}}$ (0.05, 0.09, 0.3, 0.5,
282 0.9 and 3 μM) in 1.0 m (Fig. 2a,b) and 3.2 m NaCl (Fig. 2c,d). On the left side (Fig. 2a,c),
283 uptake data are shown as $\log R_d$ versus pH_m whereas, on the right side (Fig. 2b,d), the
284 corresponding p_e versus pH_m data are given. As expected, the samples with the highest
285 $[\text{Np(V)}]_{\text{tot}}$ show the highest p_e and the lowest $\log R_d$, whereas the highest $\log R_d$ values are
286 measured at the lowest p_e and the lowest $[\text{Np(V)}]_{\text{tot}}$. Although a small amount of Fe(II)
287 contained in the illite was supposed to be responsible for the reduction of Np(V) to Np(IV)
288 (Marsac et al. (2015a)), this could not be monitored experimentally. As calculated in the latter
289 study, the amount of Fe(II) required for the reduction of Np(V) in the most concentrated
290 sample (i.e. XANES sample: $[\text{Np(V)}]_{\text{tot}} = 3 \times 10^{-4}$ M; 20 g/L illite) corresponds to about 0.08
291 % of the total amount of Fe contained in the illite. Such small fractions are very likely below
292 the detection limit of available experimental techniques.



293

294 **Figure 1.** Np sorption to illite ($\log R_d$ in $L kg^{-1}$) after 1 week contact time in 1.0 and 3.2 m NaCl versus pH_m for
 295 $[Np(V)]_{tot} = 10^{-6} M$ (a) and $5 \times 10^{-8} M$ (b). The results obtained in 0.1 m NaCl are taken from Marsac et al. (2015a)
 296 after 1 week contact time, $[Np(V)]_{tot} = 10^{-6} M$ (a) and $3 \times 10^{-8} M$ (b).

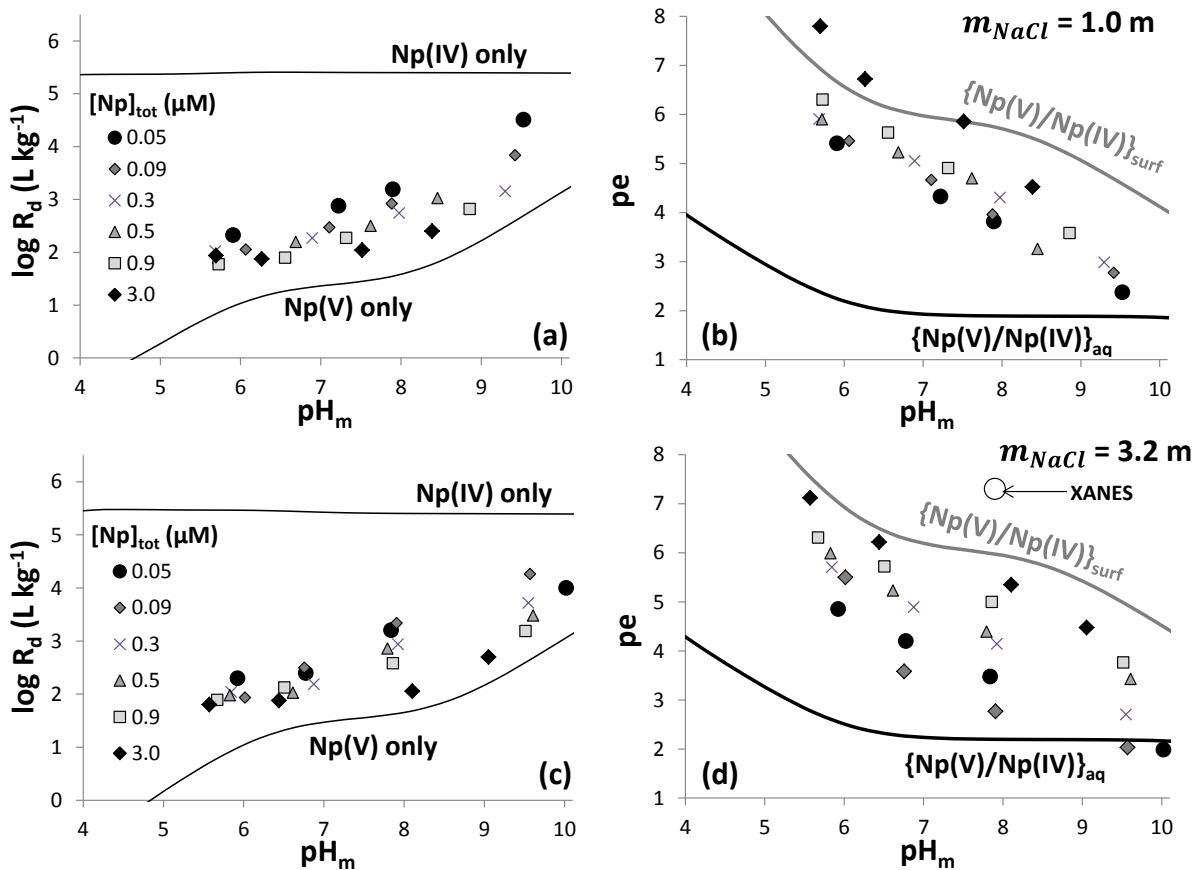
297

298 3.2. Simulation of Np(V) and Np(IV) uptake

299 Calculations are made using the 2 SPNE SC/CE model in combination with SIT and
 300 the surface complexation constants for Np(V) and Pu(IV) determined by Bradbury and
 301 Baeyens (2009b) and Banik et al. (2016), respectively, for $[NaCl/ClO_4] \leq 0.1 m$. Np(IV)
 302 sorption is considered to be identical to that of Pu(IV). The model is used to calculate the
 303 uptake of Np(V) and Np(IV) without considering redox transitions. Results are shown in
 304 figure 2a (for 1 m NaCl) and 2c (for 3.2 m NaCl). As for Pu(IV) (Marsac et al., 2017), no
 305 significant ionic strength effect on Np(IV) sorption onto illite is observed for $0.1 < m_{NaCl} <$

306 3.2 m. This is also consistent with the outcome of a previous study on Th(IV) sorption to
307 montmorillonite between 0.1 and 1 m NaClO₄ (Bradbury and Baeyens, 2005). Also the Np(V)
308 surface complexation to illite is found to be weakly affected by ionic strength for $0.1 < m_{NaCl}$
309 < 3.2 m (see also Nagasaki et al., 2016). As all metal ions, Np(V) is known to sorb to illite via
310 cation exchange at low pH (pH < 6; for Np(V)) and at pH > 6 via inner sphere complexation.
311 However, due to the small charge of the NpO₂⁺ ion, and the multiple excess of Na⁺
312 concentration, cation exchange becomes negligible and hence ionic strengths effects are not
313 pronounced. In figures 2a (for 1 m NaCl) and 2c (for 3.2 m NaCl), our experimentally
314 determined log R_d values lie between those calculated for Np(V) and Np(IV) sorption data.

315



316

317 **Figure 2.** On the left: experimental $\log R_d$ data measured after 1 week versus the pH_m for the various $[Np]_{tot}$
 318 investigated (0.05, 0.09, 0.3, 0.5, 0.9 and 3 μM ; shown as different symbols), for $m_{NaCl} = 1.0$ m (a) and 3.2 m
 319 (c). Calculated pH -edges for sorption of Np(V) and Np(IV) (no redox transition considered), respectively, are
 320 shown as lines. On the right: corresponding pH_m - pe values measured in $m_{NaCl} = 1.0$ m (b) and 3.2 m (d) for the
 321 different $[Np]_{tot}$ are shown with the same symbols as on the left. The calculated Np(V)/Np(IV) redox borderlines
 322 in solution ($\{Np(V)/Np(IV)\}_{aq}$; black line) and at the illite surface ($\{Np(V)/Np(IV)\}_{surf}$; grey line) are also shown.
 323 Error bars are not shown for clarity but uncertainties for $\log R_d$ (a,c) lie in the range of ± 0.3 and for pe (b,d) in
 324 the range of ± 0.8 . The pH - pe value for the sample analyzed by XANES ($m/V = 20$ g L^{-1} ; 3.2 m NaCl; $[Np]_{tot} =$
 325 3×10^{-4} M) is also shown (d).

326

327 3.3. pH - pe diagrams in solution and at the illite surface

328 Redox borderlines between the predominance fields of Np(V) and Np(IV) in solution
 329 (noted as $\{Np(V)/Np(IV)\}_{aq}$) are shown in figures 2b (for 1.0 m NaCl) and 2d (for 3.2 m
 330 NaCl) as black lines. The borderline between the predominance fields of Np(V) and Np(IV)
 331 species adsorbed at the surface of illite (noted as $\{Np(V)/Np(IV)\}_{surf}$) is described by:

$$332 \{Np(V)/Np(IV)\}_{surf} = \{Np(V)/Np(IV)\}_{aq} + (\log R_d(Np(IV)) - \log R_d(Np(V))) \quad (6)$$

333 and is plotted as well in figures 2b and 2d (grey lines). In eq. 6, $\{Np(V)/Np(IV)\}_{aq}$ and
334 $\{Np(V)/Np(IV)\}_{surf}$ correspond to pe values, where $[Np(V)]_{aq}/[Np(IV)]_{aq}$ and
335 $[Np(V)]_{surf}/[Np(IV)]_{surf}$ equal 1. They can vary with physico-chemical conditions (pH_m , m_{NaCl} ,
336 T , etc) in a similar way as $\log R_d(Np(IV))$ and $\log R_d(Np(V))$.

337 As shown in previous studies (Marsac et al., 2015a,b; Banik et al., 2016; Marsac et al.,
338 2017), the stability fields of surface sorbed $Np(IV)$ and $Pu(IV)$ species are extended relative to
339 those for dissolved species because of their stronger sorption relative to that of other redox
340 states (i.e. $Pu(III, V, VI)$; $Np(V)$) under the conditions investigated in those studies. For $pH < 6$,
341 at elevated ionic strength (i.e. 1.0 and 3.2 m), we find a shift of $\{Np(V)/Np(IV)\}_{surf}$ to
342 significantly higher values because $Np(V)$ sorption to illite is decreased. $Np(V)$ and $Np(IV)$
343 inner-sphere surface complexation to illite is only weakly affected by ionic strength so that
344 $\{Np(V)/Np(IV)\}_{surf}$ hardly varies between 0.1 and 3.2 m $NaCl$ for $pH > 6$.

345 By comparing the experimental pH_m-pe values and the calculated values for
346 $\{Np(V)/Np(IV)\}_{aq}$ and $\{Np(V)/Np(IV)\}_{surf}$, we expect $Np(V)$ to prevail in solution while
347 $Np(IV)$ predominantly exists as surface species. This qualitatively explains why the measured
348 Np sorption data lie between those calculated for pentavalent and tetravalent Np species.

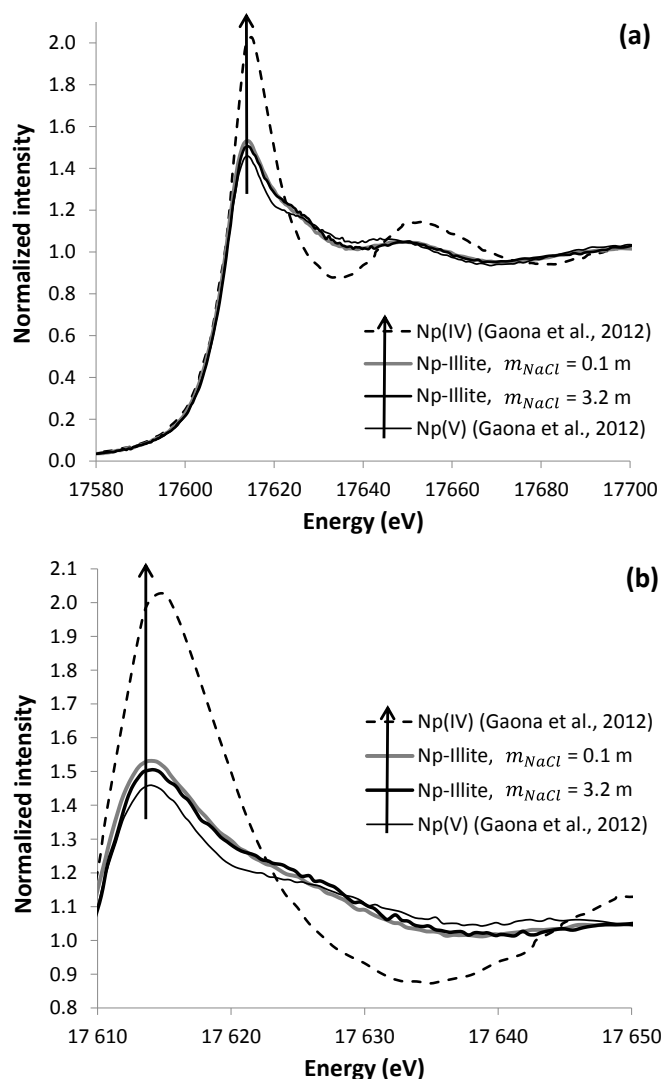
349

350 **3.4. Spectroscopic results**

351 Np redox speciation at the illite surface was further investigated by XANES for $pH_m =$
352 7.9 ($pe = 7.3 \pm 0.8$), $m/V = 20 \text{ g L}^{-1}$, 3.2 m $NaCl$ and $3 \times 10^{-4} \text{ M Np}$ (introduced as NpO_2^+). In
353 figure 3, the XANES spectrum recorded for the Np -illite sample prepared in 3.2 m $NaCl$ is
354 compared to the spectrum recorded in $m_{NaCl} = 0.1 \text{ m}$ by Marsac et al. (2015a) under similar
355 conditions ($pH_m = 7.4$; $pe = 6.8 \pm 0.8$). As explained before, phase separation was performed
356 to remove the solution from the sample. Therefore, the following analysis of spectra pertains
357 only to Np species associated to the solid phase. The Np -illite XANES spectra are compared
358 to those reported for Np^{4+} and NpO_2^+ aquo ions in 0.1 M $HClO_4$ (Gaona et al., 2012),

359 measured at the same beamline. The presence of a shoulder at 17625 eV indicates multiple
360 scattering of the outgoing Np $2p_{3/2}$ electrons along the axis of the NpO_2^+ dioxo cation. This
361 indicates the prevalence of the +V redox state in both Np-illite samples. The “white line” (WL)
362 position as well as the inflection point of Np redox states +IV and +V are similar and cannot
363 be used as a conclusive probe for Np redox speciation. However, Np(V) and Np(IV) XANES
364 show significant differences in the intensity of the WL. The WL intensity increases from the
365 NpO_2^+ aquo ion to the Np-illite sample in 0.1 m NaCl. The sample prepared in 3.2 m NaCl
366 shows intermediate intensity. As discussed in more detail in Marsac et al. (2015a) and
367 Denecke et al. (2005), the WL of Np(V) sorbed to a mineral surface will be less intense than
368 that of the Np(V) aquo-ion. Therefore, the present results indicate the presence of Np(IV). By
369 fitting the 0.1 m NaCl Np-illite XANES spectrum with a linear combination of Np(V) and
370 Np(IV) reference samples (i.e. aquo-ions), Marsac et al. (2015a) found that $14 \pm 1\%$ (error
371 provided by the Demeter Athena software; Ravel and Newville, 2005) of the adsorbed Np was
372 Np(IV) (i.e. Np(V)-to-Np(IV) concentration ratio at the illite surface $[\text{Np(V)}]_{\text{surf}}/[\text{Np(IV)}]_{\text{surf}} =$
373 6.1). Repeating the same exercise for the 3.2 m NaCl sample yields the presence of at least
374 $8 \pm 1\%$ of the Np existing as tetravalent species at the illite surface (i.e. $[\text{Np(V)}]_{\text{surf}}/[\text{Np(IV)}]_{\text{surf}}$
375 $= 11.5$). Although this value is small, it must be considered as a minimum value since the
376 aquo-ions exhibit the most intense WLs. The same exercise with either a Np(V) or a Np(IV)
377 reference, where Np is in a more condensed state (i.e. with a less intense WL), would lead to a
378 larger fraction of Np(IV) (Marsac et al., 2015a). XANES analysis, therefore, yields a similar
379 result compared to what has been obtained for the experiment at low ionic strength and
380 provides a clear indication for partial reduction of Np(V), also at elevated ionic strength.
381 Using experimental p_e and spectroscopically determined $[\text{Np(V)}]_{\text{surf}}/[\text{Np(IV)}]_{\text{surf}}$ values, we
382 find that $\{\text{Np(V)}/\text{Np(IV)}\}_{\text{surf}} = 6.0$ (for $m_{\text{NaCl}} = 0.1$) and 6.2 (for $m_{\text{NaCl}} = 3.2$). These values
383 compare very well with $\{\text{Np(V)}/\text{Np(IV)}\}_{\text{surf}} = 5.9$ (for both 0.1 and 3.2 m NaCl), as
384 determined by modeling (see e.g. the grey lines in Fig. 2b,d). This further confirms that the

385 Np(V)-Np(IV) redox transition at the illite surface is not substantially affected by ionic
386 strength.



387

388 **Figure 3.** (a) Np L₃-XANES measured for Np-illite samples ($[\text{Np}]_{\text{tot}} = 3 \times 10^{-4} \text{ M}$, $m/V = 20 \text{ g L}^{-1}$) prepared in 0.1
389 m NaCl ($\text{pH}_m = 7.4$; $\text{pe} = 6.8$; Marsac et al., 2015a) and 3.2 m NaCl ($\text{pH}_m = 7.9$; $\text{pe} = 7.3$; present study).
390 Reference XANES of aqueous Np(IV) and Np(V) in 1 M HClO₄ from Gaona et al. (2012) are shown for
391 comparison. Arrows highlight the partial Np(V) reduction to Np(IV) in the present study. The area between
392 17610 and 17650 eV is enlarged in (b). Results of the linear combination fit are shown in the supporting
393 information (Figure S1).

394

395

4. DISCUSSION

4.1. Effects of pH_m , pe and m_{NaCl} on Np sorption to illite

Because Np uptake on illite is sensitive to pH_m and pe , it appears difficult to study in detail the effect of a third parameter, namely m_{NaCl} . Figure 4 shows data for experimentally determined $\log R_d$ plotted versus pe for $m_{NaCl} = 0.1, 1.0$ and 3.2 . It is obvious that there is a strong correlation between R_d and pe showing that increasing the pe from 2 to 6 reduces R_d by ~ 3 orders of magnitude. In so far “ pe edges” ($\log R_d$ plotted vs. pe) are more informative than the “ pH edges” in Figures 2a and 2c ($\log R_d$ vs. pH). It appears that pe is the more relevant parameter determining Np retention under given conditions. A few experimental data do not fit into the trend and have been excluded from figure 4: (i) sorption data obtained at $pH_m < 6$ show a significant pH dependence because the Np(V)/Np(IV) borderlines in this range clearly evolve with pH (see Fig. 2b,d); (ii) at quite high pe values, where Np(V) prevails in solution and at the illite surface, the influence of pH on Np sorption is of course dominant (see the pH -edges of Np(V) in Fig. 2a,c). The exclusion of data points amount to $\sim 20\%$ of the complete data set, and make sure that, for the selected data, pH has no significant effect.

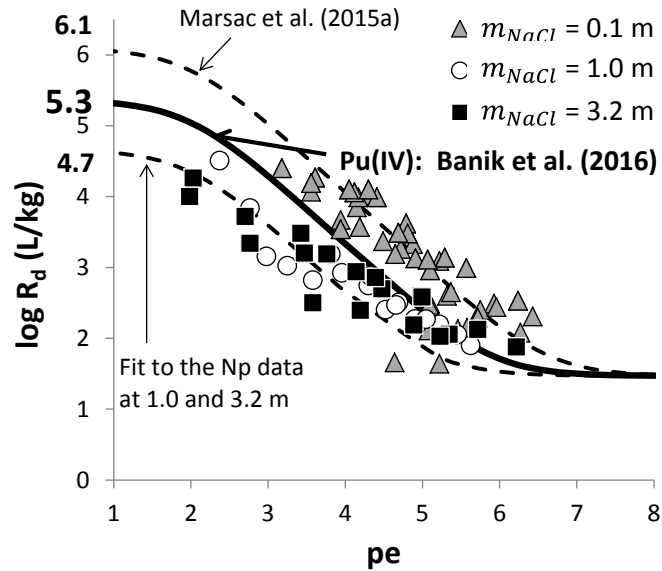
Figure 4 seems to suggest that Np sorption to illite is stronger in 0.1 than in 1.0 and 3.2 m NaCl at least for $pe < 4.5$, an issue that does not occur on Figure 1. Recent experimental investigations did not show significant influence of ionic strength neither on tetravalent actinide ion ($I = 0.1 - 3.2$ m; Bradbury and Baeyens, 2005; Marsac et al., 2017; results of both studies on Th(IV) and Pu(IV) sorption are shown in the supporting information) nor on Np(V) sorption to illite via inner-sphere surface complexation ($I = 0.1$ to 4.6 M; Nagasaki et al., 2016). Moreover, our XANES results suggest no ionic strength effect on Np(V)-Np(IV) redox transition at the illite surface. In fact, the interpretation of the Np-illite results is strongly affected by the experimental pe . Unlike Np, Th(IV) is not a redox sensitive metal ion and its sorption on illite is independent of the ionic strength within the experimental uncertainties.

421 The same independency of the ionic strength is observed for Pu(IV) illite uptake. From these
422 results it would appear difficult to assume, that the ionic strength has no significant influence
423 on the Np(IV) uptake, although trends in average values could suggest such effects. Therefore,
424 it is more probable that the variations of Np-illite uptake data are due to the uncertainties of
425 experimental pe measurements.

426 To highlight the consistency between Np-illite and Pu-illite sorption data in 0.1, 1.0
427 and 3.2 m NaCl (Banik et al., 2016; Marsac et al., 2017; present study), simulations are made
428 with the 2 SPNE SC/CE model for $\text{pH}_m = 7$ and the results are plotted in Figure 4. This pH_m
429 value is arbitrarily chosen because insignificant pH_m effect is expected for the selected dataset,
430 as explained above. The surface complexation constant for Np(IV) given by Marsac et al.
431 (2015a) (Table S3) describes sorption data determined for low ionic strength accurately, but
432 overestimates sorption when comparing with experimental data determined in this study. In
433 this case, $\log R_d(\text{Np(IV)}) = 6.1$ (i.e. $\log R_d$ values extrapolated to pe values where all Np(V)
434 in the system is reduced to Np(IV) in solution and at the illite surface). Adjusting model
435 parameters to fit our data in 1.0 and 3.2 m NaCl using PhreePlot leads to $\log R_d(\text{Np(IV)}) = 4.7$
436 (corresponding surface complexation constants are given in Table S3). In average, the model
437 would give $\log R_d(\text{Np(IV)}) = 5.4 \pm 0.7$ (which is also determined by Phreeplot when using the
438 complete dataset in 0.1, 1.0 and 3.2 m NaCl; Table S3). This average value is in excellent
439 agreement with $\log R_d(\text{Pu(IV)}) = 5.3 \pm 0.3 \text{ L kg}^{-1}$ determined by Marsac et al. (2017) for $0.1 <$
440 $m_{\text{NaCl}} < 3.2 \text{ m}$. Figure 4 shows that calculated $\log R_d$ evolves linearly with pe for
441 intermediate pe values (for $\{\text{Np(V)/Np(IV)}\}_{\text{aq}} < \text{pe} < \{\text{Np(V)/Np(IV)}\}_{\text{surf}}$, all the selected data
442 are within this range in Figure 4). Therefore, an error of ± 0.8 on pe leads to an error of ± 0.8
443 on the calculated $\log R_d$ value, which compares well with the error on determined \log
444 $R_d(\text{Np(IV)})$ using Np-illite data at 0.1, 1 and 3.2 m NaCl (± 0.7). These results suggest that it
445 is reasonable to impose surface complexation constants for Np(IV) equal to those of Pu(IV)

446 and to attribute the trend of average Np-illite uptake with ionic strength effects to
 447 uncertainties in pe.

448



449

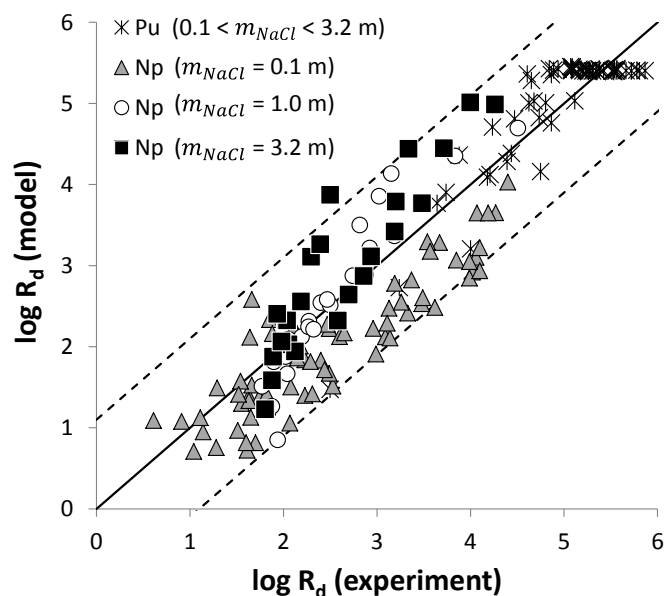
450 **Figure 4.** Np-illite sorption datasets from Marsac et al. (2015a; $m_{NaCl} = 0.1$ m) and the present study ($m_{NaCl} =$
 451 1.0 and 3.2 m) are plotted as $\log R_d$ versus pe. Lines are calculations made with the 2 SPNE SC/CE model for
 452 $pH_m = 7$ using the surface complexation constants determined by Marsac et al. for Np(IV) (2015a; top dotted
 453 line), Banik et al. for Pu(IV) (2016; bold line) or fitting these constants to the 1.0 and 3.2 m NaCl data (bottom
 454 dotted curve). The corresponding $\log R_d(Np(IV))$ is given on the y-axis.

455

456 **4.2. Modeling An(III,IV,V) sorption to illite as a function of pH_m , pe and m_{NaCl}**

457 Values of $\log R_d$ are calculated for all the presently investigated conditions (including
 458 the conditions of Marsac et al., 2015a) using the experimental pH_m and pe values. The model
 459 results are plotted versus the experimental $\log R_d$ in Figure 5. The results of Banik et al. (2016;
 460 0.1 m NaCl) and Marsac et al. (2017; 1.0 and 3.2 m NaCl), involving the Pu(IV)/Pu(III)
 461 couple, are also included. The 1:1 line shows the good agreement between model and
 462 experiment. Deviations of ± 1.1 $\log R_d$ unit are shown as dotted lines. This error for the
 463 calculated $\log R_d$ accounts for both the error on pe (± 0.8) and on experimental $\log R_d$ (± 0.3).
 464 For a wide range of pH_m , $[Np/Pu]_{tot}$, m_{NaCl} and pe investigated in these different studies (i.e.
 465 179 experimental $\log R_d$ values) the discrepancies between model and the experimental

466 results rarely exceed 1.1 log R_d unit. The mean value of the deviation between experimental
 467 and calculated log R_d values is 0.42. It is important to note that sorption data are highly
 468 sensitive to the redox conditions and pe measurements are associated with considerable
 469 uncertainties. We nevertheless conclude that the combination of (i) the 2 SPNE SC/CE model,
 470 (ii) SIT and (iii) the approach developed by Marsac et al. (2015a,b), which accounts for redox
 471 equilibria and the stability of surface species, allows to reasonably model actinide(III,IV,V)
 472 uptake by illite as a function of pH_m , pe and m_{NaCl} up to highly saline conditions.
 473



474
 475 **Figure 5.** Modelled versus experimental log R_d values for Np (data from this study and Marsac et al., 2015a) and
 476 Pu in $0.1 < m_{NaCl} < 3.2$ m (data from Banik et al., 2016; Marsac et al., 2017). The 1:1 (solid) line is associated
 477 with an uncertainty of ± 1.1 log R_d units (dashed lines).
 478

479 4. CONCLUSIONS

480 In agreement with previous studies performed at low ionic strength (Marsac et al.,
 481 2015a), Np sorption increases with decreasing redox potential also at high m_{NaCl} (up to 3.2
 482 m). Using a combined batch sorption, spectroscopic and geochemical modeling approach, the
 483 strong interaction between Np and illite is attributed to the partial reduction of Np(V) to

484 Np(IV) at the illite surface driven by the higher thermodynamic stability of Np(IV) surface
485 complexes as compared to Np(V) surface species. By the combination of the 2 SPNE SC/CE
486 model with SIT, it is possible to reproduce experimentally obtained overall Np uptake data for
487 illite as a function of pH_m , pe and m_{NaCl} using a single set of parameters. The ionic strength
488 has a relatively small impact on sorption of both Np(V) and Np(IV). Main parameters driving
489 the sorption behavior of redox sensitive actinides are pH_m and pe .

490 Notably the role of the redox potential on the uptake of redox sensitive actinides on
491 minerals is to be considered when applying laboratory derived conditional R_d values for
492 performance safety assessment purposes. The applicability of such data is only justified, if
493 redox conditions in laboratory experiments and those expected in the real system are identical.
494 This is not always the case as extraction of natural materials from deep environments,
495 transport to the laboratory and experimental handling are technically challenging and redox
496 conditions may change due to e.g. access of oxygen. However, if the pH and redox potentials
497 of *in situ* and laboratory conditions are known, mechanistic models as proposed here, are
498 capable of assessing the overall uptake of redox sensitive actinides by natural adsorbents with
499 reasonable accuracy. In agreement with recent studies, the use of non-electrostatic models
500 appears suitable for the prediction of metal ion sorption to various types of surfaces even at
501 elevated ionic strength, e.g. marine microalgae (Zoll and Schjif, 2012), bacteria (Ams et al.,
502 2013), illite (Schnurr et al., 2015; Marsac et al., 2017) or smectite (Schnurr et al., 2015).
503 Accordingly, the 2 SPNE SC/CE model is a reliable predictive tool for performance safety
504 assessment for clays even under elevated saline conditions.

505

506 **ACKNOWLEDGEMENTS**

507 This work was financed by the Federal Ministry of Economic Affairs and Energy
508 (Germany) under contracts No. 02E10206 and 02E10961. The research leading to these

509 results has received funding from the European Union's European Atomic Energy
510 Community's (Euratom) Seventh Framework Program FP7/2007-2011 under grant agreement
511 n° 249624 (CATCLAY project).

512

513 **Supporting Information Available**

514 Additional material is provided in the supporting information section.

515

516 **REFERENCES**

- 517 Altmaier M., Gaona X. and Fanghänel T. (2013) Recent advances in aqueous actinide
518 chemistry and thermodynamics. *Chem. Rev.* **113**, 901-943.
- 519 Altmaier M., Gaona X., Fellhauer D. and Buckau G. (2010) Intercomparison of redox
520 determination methods on designed and near-neutral aqueous systems. KIT-SR 7572,
521 Karlsruhe Institute of Technology, Karlsruhe.
- 522 Altmaier M., Metz V., Neck V., Müller R. and Fanghänel Th. (2003) Solid-liquid equilibria of
523 $\text{Mg}(\text{OH})_{2(\text{cr})}$ and $\text{Mg}_2(\text{OH})_3\text{Cl}\cdot 4\text{H}_2\text{O}_{(\text{cr})}$ in the system Mg-Na-H-OH-Cl-H₂O at 25°C.
524 *Geochim. Cosmochim. Acta* **67**, 3595–3601.
- 525 Ams D. A., Swanson J. S., Szymanowski J. E. S., Fein J. B., Richmann M. and Reed D. T.
526 (2013) The effect of high ionic strength on neptunium (V) adsorption to a halophilic
527 bacterium. *Geochim. Cosmochim. Acta* **110**, 45–57.
- 528 Andra, Dossier 2005 Synthèse Évaluation de la faisabilité du stockage géologique en
529 formation argileuse. 2005, Agence nationale pour la gestion des déchets radioactifs
530 (Andra): Châtenay-Malabry, France. p. 241.
- 531 Banik N. L., Marsac R., Lützenkirchen J., Diascorn A., Bender K. Marquardt C. M. and
532 Geckeis H. (2016) Sorption and redox speciation of plutonium on illite. *Environ. Sci.*
533 *Technol.* **50**, 2092–2098.
- 534 Bradbury M. H. and Baeyens B. (2005) Modelling the sorption of Mn(II), Co(II), Ni(II),
535 Zn(II), Cd(II), Eu(III), Am(III), Sn(IV), Th(IV), Np(V) and U(VI) on montmorillonite:
536 Linear free energy relationships and estimates of surface binding constants for some
537 selected heavy metals and actinides. *Geochim. Cosmochim. Acta* **69**, 875–892.
- 538 Bradbury M. H. and Baeyens B. (2009a) Sorption modelling on illite Part I: Titration
539 measurements and the sorption of Ni, Co, Eu and Sn. *Geochim. Cosmochim. Acta.* **73**,
540 990–1003.
- 541 Bradbury M. H. and Baeyens B. (2009b) Sorption modeling on illite Part II: actinide sorption
542 and linear free energy relationships. *Geochim. Cosmochim. Acta.* **73**, 1004–1013.
- 543 Bradbury M. H. and Baeyens B. (2011) Predictive sorption modelling of Ni(II), Co(II),
544 Eu(III), Th(IV) and U(VI) on MX-80 bentonite and Opalinus Clay: A “bottom-up”
545 approach, *Appl. Clay Sci.* **52**, 27–33.
- 546 Brendebach B., Banik N. L., Marquardt C. M., Rothe J., Denecke M. and Geckeis H. (2009)
547 X- ray absorption spectroscopic study of trivalent and tetravalent actinides in solution at
548 varying pH value. *Radiochim. Acta* **97**, 701–708.
- 549 Brewitz W. (1980) Zusammenfassender Zwischenbericht, GSF T 114.
- 550 Chen Z., Montavona G., Guo Z., Wang X., Razafindratsima S., Robinet J. C., Landesmana C.
551 (2014) Approaches to surface complexation modeling of Ni(II) on Callovo-Oxfordian
552 clayrock. *Appl. Clay Sci.* **101**, 369–380.
- 553 Ciavatta L. (1980). The specific interaction theory in the evaluating ionic equilibria. *Ann.*
554 *Chim.* **70**, 551–562.

- 555 Denecke M. A., Dardenne K. and Marquardt C. M. (2005) Np(IV)/Np(V) valence
556 determinations from Np L3 edge XANES/EXAFS. *Talanta* **65**, 1008–1014.
- 557 Fritz P. and Frapé S. K. (1982). Saline groundwaters in the Canadian shield – a first overview.
558 *Chem. Geol.* **36**, 179–190.
- 559 Fröhlich D. R., Amayri S., Drebert J. and Reich T. (2011) Sorption of neptunium(V) on
560 Opalinus Clay under aerobic/anaerobic conditions. *Radiochim. Acta* **99**, 71–77.
- 561 Fröhlich D. R., Amayri S., Drebert J., Grolimund D., Huth J., Kaplan U., Krause J. and Reich
562 T. (2012) Speciation of Np(V) uptake by Opalinus Clay using synchrotron microbeam
563 techniques. *Anal. Bioanal. Chem.* **404**, 2151–2162.
- 564 Gaines G. I. and Thomas H. C. (1953) Adsorption studies on clay minerals. II. A formulation
565 of the thermodynamics of exchange adsorption. *J. Phys. Chem.* **21**, 714–718.
- 566 Gaona X., Tits J., Dardenne K., Liu X., Rothe J., Denecke M. A., Wieland E. and Altmaier M.
567 (2012) Spectroscopic investigations of Np(V/VI) redox speciation in hyperalkaline
568 TMA-(OH, Cl) solutions. *Radiochim. Acta* **100**, 759–770.
- 569 Gaucher E., Robelin C., Matray J. M., Négrel G., Gros Y., Heitz J. F., Vinsot A., Rebours H.,
570 Cassagnabère A. and Bouchet A. (2004) ANDRA underground research laboratory:
571 interpretation of the mineralogical and geochemical data acquired in the Callovian–
572 Oxfordian formation by investigative drilling. *Phys. Chem. Earth* **29**, 55–77.
- 573 Geckeis H., Lützenkirchen J., Polly R., Rabung T. and Schmidt M. (2013) Mineral–water
574 interface reactions of actinides. *Chem. Rev.* **13** (2), 1016–1062.
- 575 Graser C.-H., Banik N. L., Bender K. A., Marquardt C. M., Marsac R., Monytoy, V. and
576 Geckeis H. (2015) Sensitive Redox speciation of elements relevant to nuclear waste
577 disposal by Capillary Electrophoresis hyphenated to inductively coupled plasma sector
578 field mass spectrometry. *Anal. Chem.* **87**, 9786–94.
- 579 Guillaumont R., Fanghänel Th., Fuger J., Grenthe I., Neck V., Palmer D. A. and Rand M. H.
580 (2003) Update on the chemical thermodynamics of Uranium, Neptunium, Plutonium,
581 Americium and Technetium, Mompean, F.J., Domenech-Orti, C., Ben-Said, K.,
582 OECD/NEA Data Bank, Eds., vol. 5 of Chemical Thermodynamics, Elsevier,
583 Amsterdam.
- 584 Kim J. I. (1986) Chemical behaviour of transuranic elements in natural aquatic systems. In:
585 Handbook on the Physics and Chemistry of the Actinides. (Freeman, A. J., ed.) Elsevier
586 Science Publishers, B. V., Amsterdam p. 413.
- 587 Kinniburgh D. G. and Cooper D. M. (2009) PhreePlot: Creating graphical output with
588 PHREEQC. <<http://www.phreeplot.org>>.
- 589 Kirsch R., Fellhauer D., Altmaier M., Neck V., Rossberg A., Fanghänel Th., Charlet L. and
590 Scheinost A. C. (2011) Oxidation state and local structure of plutonium reacted with
591 magnetite, mackinawite, and chukanovite. *Environ. Sci. Technol.* **45**, 7267–7274
- 592 Lauber M., Baeyens B. and Bradbury M. H. (2000) Physico-chemical characterisation and
593 sorption measurements of Cs, Sr, Ni, Eu, Th, Sn and Se on Opalinus Clay from Mont
594 Terri. PSI Technical Report 00-10, Paul Scherrer Institut, Villigen/Switzerland

- 595 Lázár K. and Máthé Z. (2012) Claystone as a potential host for nuclear waste storage, in
 596 “Clay minerals in nature - Their characterization, modification and application.”, Marta
 597 Valaskova (Ed.), InTech, ISBN 978-953-51-0738-5.
- 598 Marsac R., Banik N. L., Diascorn A., Kupcik T., Lützenkirchen J., Marquardt C. M., Schäfer
 599 T., Schild D., Rothe J., Dardenne K. and Geckeis H. (2015a) Neptunium redox
 600 speciation at the illite surface. *Geochim. Cosmochim. Acta* **152**, 39–51.
- 601 Marsac R., Banik N. L., Lützenkirchen J., Buda R. A., Kratz J. V. and Marquardt C. M.
 602 (2015b) Modeling plutonium sorption to kaolinite: accounting for redox equilibria and
 603 the stability of surface species. *Chem. Geol.* **400**, 1–10.
- 604 Marsac R., Banik N. L., Lützenkirchen J., Diascorn A., Bender K., Marquardt C. M. and
 605 Geckeis H. (2017) Sorption and redox speciation of plutonium on illite under highly
 606 saline conditions. *J. Coll. Int. Sci.* **485**, 59–64.
- 607 Nagasaki S., Saito T. and Yang T. T. (2016) Sorption behavior of Np(V) on illite, shale and
 608 MX-80 in high ionic strength solutions. *J. Radioanal. Nucl. Chem.*, **308**, 143–153.
- 609 Nagra (2002) Project opalinus clay: safety report. Demonstration of disposal feasibility
 610 (Entsorgungsnachweis) for spent fuel, vitrified high-level waste and long-lived
 611 intermediate-level waste. Nagra Technical Report NTB 02-05, Nagra, Wetingen,
 612 Switzerland.
- 613 OECD/NEA (2008) Radioactive waste management committee: “Collective statement on
 614 moving forward to geological disposal of radioactive waste“, ISBN 978-92-64-99057-
 615 9.
- 616 Ondraf (2001) SAFIR 2: safety assessment and feasibility interim report 2. NIROND-2001-06
 617 E. Ondraf, Brussels.
- 618 Parkhurst D. L. and Appelo C. A. J. (1999) User's guide to PHREEQC (Version 2) – a
 619 computer program for speciation, batch reaction, one-dimensional transport and inverse
 620 geochemical calculation. Water-resources Investigation Report 99-4259, USGS, Denver,
 621 Colorado, p. 312.
- 622 Pearson F. J., Tournassat C. and Gaucher E. C. (2011) Biogeochemical processes in a clay
 623 formation in situ experiment: Part E – Equilibrium controls on chemistry of pore water
 624 from the Opalinus Clay, Mont Terri Underground Research Laboratory, Switzerland.
 625 *Appl. Geochem.* **26**, 990–1008.
- 626 Pitzer K. S. (1991). Activity Coefficients in Electrolyte Solutions, CRC Press, Boca Raton.
- 627 Ravel B. and Newville M. (2005) ATHENA and ARTEMIS: data analysis for X-ray
 628 absorption spectroscopy using IFEFFIT. *J. Synchrotron Radiat.* **12**, 537–541.
- 629 Rothe J., Butorin S., Dardenne K., Denecke M. A., Kienzler B., Löble M., Metz V., Seibert A.,
 630 Steppert M., Vitova T., Walther C. and Geckeis H. (2012) The INE-Beamline for
 631 actinide science at ANKA. *Rev. Sci. Instrum.* **83**, 043105.
- 632 Rothe J., Denecke M. A., Dardenne K. and Fanghänel T. (2006) The INE-beamline for
 633 actinide research at ANKA. *Radiochim. Acta.* **94**, 691–696.

- 634 Schijf J. and Ebling A. M. (2010) Investigation of the ionic strength dependence of *Ulva*
635 *lactuca* acid functional group pK_{as} by manual alkalimetric titrations. *Environ. Sci.*
636 *Technol.* **44**, 1644–1649
- 637 Schnurr A., Marsac R., Kupcik T., Rabung T., Lützenkirchen J. and Geckeis H. (2015)
638 Sorption of Cm(III) and Eu(III) onto clay minerals under saline conditions: Batch
639 adsorption, Laser-fluorescence spectroscopy and modeling. *Geochim. Cosmochim. Acta*
640 **151**, 192–202.
- 641 Sjoblom R. and Hindman J.C. (1951) Spectrophotometry of neptunium in perchloric acid
642 solutions. *J. Am. Chem. Soc.* **73**(4), 1744–1751.
- 643 Vilks P. (2011) Sorption of selected radionuclides on sedimentary rocks in saline conditions –
644 Literature review. NWMO TR-2011-12, Atomic Energy of Canada Limited, Toronto,
645 Ontario, Canada.
- 646 Zoll A. M. and Schijf J. (2012) A surface complexation model of YREE sorption on *Ulva*
647 *lactuca* in 0.05–5.0 M NaCl solutions. *Geochim. Cosmochim. Acta* **97**, 183–199.
- 648

649 **Figure caption**

650 **Figure 1.** Np sorption to illite ($\log R_d$ in $L\ kg^{-1}$) after 1 week contact time in 1.0 and 3.2 m
651 NaCl versus pH_m for $[Np(V)]_{tot} = 10^{-6}$ M (a) and 5×10^{-8} M (b). The results obtained in 0.1 m
652 NaCl are taken from Marsac et al. (2015a) after 1 week contact time, $[Np(V)]_{tot} = 10^{-6}$ M (a)
653 and 3×10^{-8} M (b).

654 **Figure 2.** On the left: experimental $\log R_d$ data measured after 1 week versus the pH_m for the
655 various $[Np]_{tot}$ investigated (0.05, 0.09, 0.3, 0.5, 0.9 and 3 μ M; shown as different symbols),
656 for $m_{NaCl} = 1.0$ m (a) and 3.2 m (c). Calculated pH-edges for sorption of Np(V) and Np(IV)
657 (no redox transition considered), respectively, are shown as lines. On the right: corresponding
658 pH_m -pe values measured in $m_{NaCl} = 1.0$ m (b) and 3.2 m (d) for the different $[Np]_{tot}$ are
659 shown with the same symbols as on the left. The calculated Np(V)/Np(IV) redox borderlines
660 in solution ($\{Np(V)/Np(IV)\}_{aq}$; black line) and at the illite surface ($\{Np(V)/Np(IV)\}_{surf}$; grey
661 line) are also shown. Error bars are not shown for clarity but uncertainties for $\log R_d$ (a,c) lie
662 in the range of ± 0.3 and for pe (b,d) in the range of ± 0.8 . The pH-pe value for the sample
663 analyzed by XANES ($m/V = 20\ g\ L^{-1}$; 3.2 m NaCl; $[Np]_{tot} = 3 \times 10^{-4}$ M) is also shown (d).

664 **Figure 3.** (a) Np L_3 -XANES measured for Np-illite samples ($[Np]_{tot} = 3 \times 10^{-4}$ M, $m/V = 20\ g$
665 L^{-1}) prepared in 0.1 m NaCl ($pH_m = 7.4$; pe = 6.8; Marsac et al., 2015a) and 3.2 m NaCl (pH_m
666 = 7.9; pe = 7.3; present study). Reference XANES of aqueous Np(IV) and Np(V) in 1 M
667 $HClO_4$ from Gaona et al. (2012) are shown for comparison. Arrows highlight the partial Np(V)
668 reduction to Np(IV) in the present study. The area between 17610 and 17650 eV is enlarged
669 in (b). Results of the linear combination fit are shown in the supporting information (Figure
670 S1).

671 **Figure 4.** Np-illite sorption datasets from Marsac et al. (2015a; $m_{NaCl} = 0.1$ m) and the
672 present study ($m_{NaCl} = 1.0$ and 3.2 m) are plotted as $\log R_d$ versus pe. Lines are calculations
673 made with the 2 SPNE SC/CE model for $pH_m = 7$ using the surface complexation constants
674 determined by Marsac et al. for Np(IV) (2015a; top dotted line), Banik et al. for Pu(IV) (2016;
675 bold line) or fitting these constants to the 1.0 and 3.2 m NaCl data (bottom dotted curve). The
676 corresponding $\log R_d(Np(IV))$ is given on the y-axis.

677 **Figure 5.** Modelled versus experimental $\log R_d$ values for Np (data from this study and
678 Marsac et al., 2015a) and Pu in $0.1 < m_{NaCl} < 3.2$ m (data from Banik et al., 2016; Marsac et
679 al., 2017). The 1:1 (solid) line is associated with an uncertainty of ± 1.1 $\log R_d$ units (dashed
680 lines).

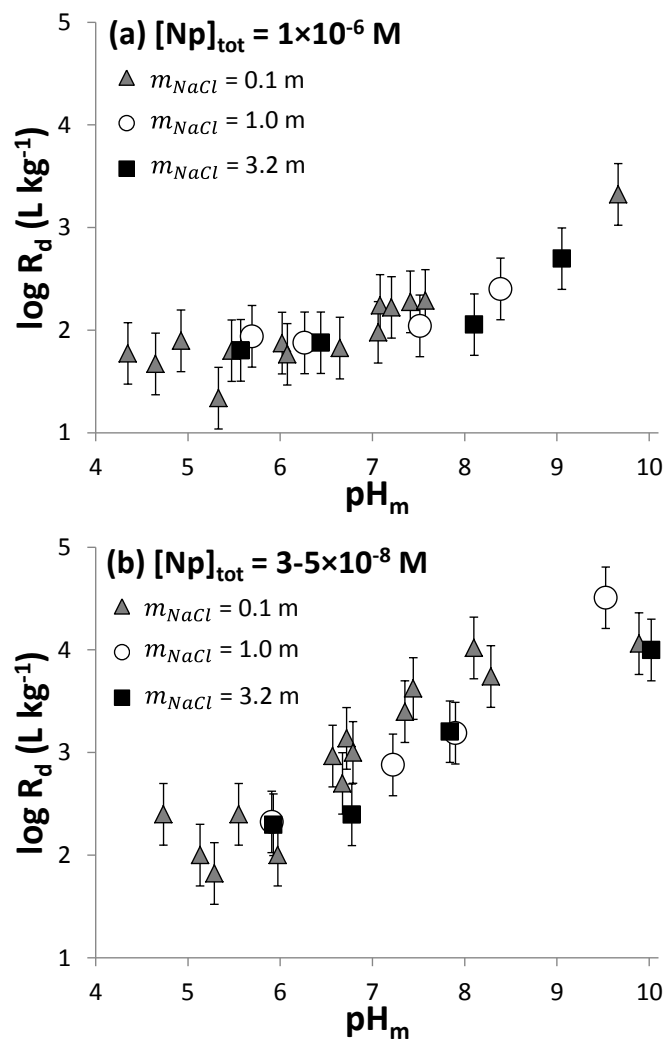
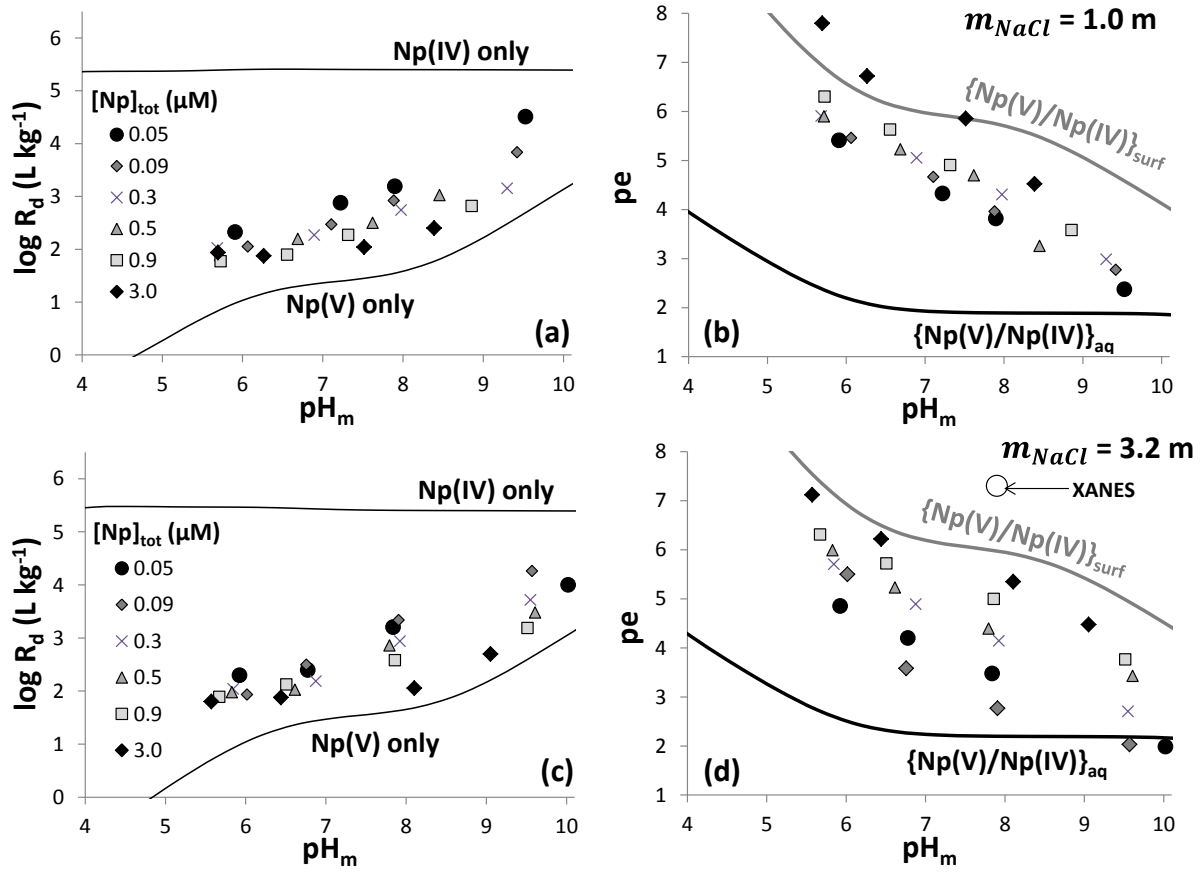


Figure 1

681

682

683

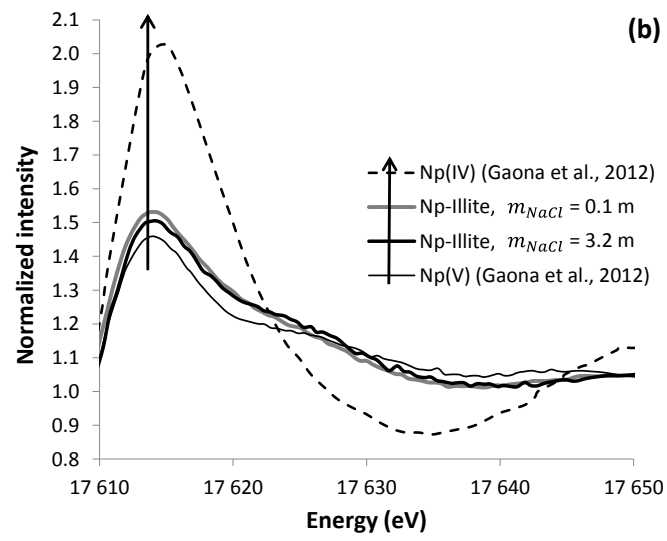
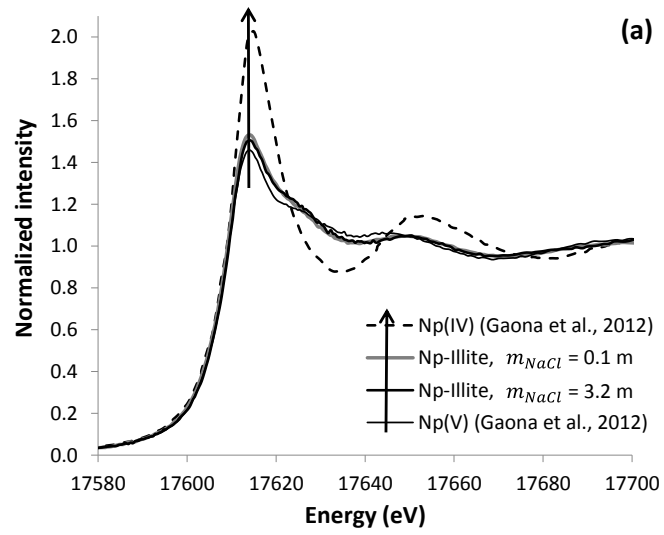


684

685

686

Figure 2



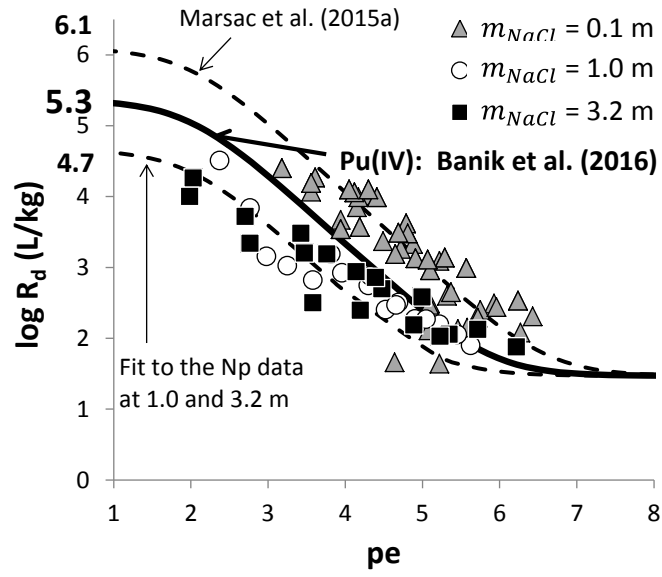
687

688

689

Figure 3

690

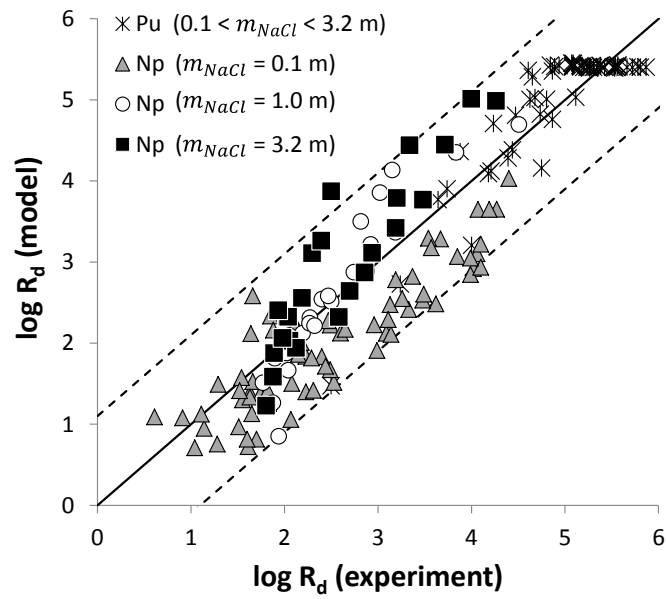


691

692

Figure 4

693



694

695

Figure 5